ABSTRACT

Title of Document:	THIN-FILAMENT PYROMETRY WITH A DIGITAL STILL CAMERA
	Jignesh D. Maun, Master of Science, 2006
Directed By:	Peter B. Sunderland, Assistant Professor, Department of Fire Protection Engineering

A novel thin-filament pyrometer is presented here. It involves a consumer-grade color digital still camera with a charged-couple device sensor with 3008×2000 pixels and 12 bits per color plane. A blue Schott filter and custom white balance were used to yield similar red, green and blue intensities along the fibers. SiCO fibers with diameters of 13.9 μm were used and scanning-electron microscopy revealed the fibers to be uniform. Measurements were performed in a methane/air coflowing laminar jet diffusion flame with a luminosity length of 72 mm. Calibration of the pyrometer was accomplished with B-type thermocouple measurements. The camera was found to be well suited to thin-filament pyrometry. The pyrometry measurements yielded gas temperatures in the range of $1350 - 2200$ K with an estimated uncertainty of ± 60 K, a relative temperature resolution of ± 0.215 K, a spatial resolution of 42 μm and a temporal resolution of 0.66 ms. Fiber aging had no effect on the results. Soot deposition was less problematic for the pyrometer than for the thermocouple.

THIN-FILAMENT PYROMETRY WITH A DIGITAL STILL CAMERA

By

Jignesh D. Maun

Thesis submitted to the Faculty of the Graduate School of the
University of Maryland, College Park, in partial fulfillment
of the requirements for the degree of
Master of Science
2006

Advisory Committee:
Professor Peter B. Sunderland, Chair
Professor André W. Marshall
Professor James G. Quintiere

Dedication

To my Parents, Sister and Larry.

Acknowledgments

Table of Contents

List of Tables

List of Figures

Nomenclature

A surface area

B blue intensity

c_p specific heat

d cylinder diameter

G green intensity

h convection heat transfer coefficient

k thermal conductivity

m probe mass

Nu Nusselt number

Pe Peclet number

Pr Prandtl number

R red intensity

Re Reynolds number

T temperature

V velocity

x x pixel coordinate, distance along probe

y y pixel coordinate

Greek Symbols

α thermal diffusivity

ε graybody emissivity

ρ density

σ Stefan-Boltzmann constant

τ time constant

v kinematic viscosity

Subscripts

est   estimated

fiber   fiber

gas   gas

s   solid

TC   thermocouple

∞ far-field conditions

Chapter 1: Introduction

Temperature is among the most commonly measured and predicted quantities in combustion research. Many methods are used to measure temperature owing to diverse flame configurations and cost and time constraints. The temperature diagnostic considered here is thin-filament pyrometry (TFP). TFP provides fast thermal response times and temperatures along lines with good spatial and temporal resolution. This work seeks to develop an accurate TFP system using an inexpensive camera.

TFP involves measuring the radiative emissions of a thin fiber in a flame or other hot gas. Temperatures can then be determined from the emissions. TFP was first used by Goss, Vilimpoc and co-workers [1-5] following the development by Ferguson and Keck [6] of a hot-wire pyrometer. The initial TFP systems [1-5] used 15 μm β-SiC fibers, InGaAs point detectors (sensitive to wavelengths of 900 – 1600 nm), rotating mirrors and calibration using a steady flame of known temperature. Other researchers also have performed TFP using single-element infrared detectors using either a monochromator or rotating mirrors (or prisms) or traversable flames (or optics) [7-14].

The use of cameras for TFP was introduced by Pitts and co-workers [15,16]. They performed TFP using a cooled 16-bit charge-coupled device (CCD) video camera sensitive to visible and near-infrared light and an imaging area of 540 × 61 pixels. This obviated the rotating mirror and its alignment complications. It also facilitated correcting the signal to account for luminosity from soot and hot gases. Others too have used cooled CCD cameras for TFP, such as a 330 × 1100 pixel 16 bit

camera [17], but these cameras are costly and have limited pixel counts. A consumer-grade digital still camera with 1712 × 1368 pixels addressed the cost issue, but was limited to 8 bits and was used only for qualitative TFP [18]. Another 8-bit CCD camera, of unspecified pixel dimensions, was used by Bundy et al. [19]. As a part of a larger study, Russo and Gomez [20] used 320 × 240 infrared camera in the TFP measurements.

A Nikon D70 digital still camera, similar to the Nikon D100 used here, was used for soot pyrometry by Connelly et al. [21]. In this study, the camera was found to be linear and repeatable and to be adequate for quantitative soot pyrometry.

TFP does have its limitations. One limitation is that oxidation of the fibers in the flame can lead to breakage of the fibers. Inserting fibers in the flame is intrusive and is practical only if the fibers are in the line of sight of the camera. Generally, TFP is more labor intensive than thermocouple measurements in terms of data processing.

Given the extensive past interest in TFP and the advent of inexpensive digital still cameras, the primary objective of this work is to evaluate the suitability of such a camera for TFP. Additional objectives are to:

(1)   Examine SiCO fibers under a scanning electron microscope (SEM) to evaluate surface uniformity, measure mean diameter, and evaluate the effects of aging on these observations.

(2)   Evaluate the shot-to-shot and fiber-to-fiber repeatability.

(3)   Evaluate whether TFP can be used reliably in flame regions with light soot loading.

The present TFP system is calibrated using thermocouple measurements in a methane/air coflowing gas jet diffusion flame.

Chapter 2: Experimental Methodology

This chapter describes the experimental setup used in the present TFP measurements. Descriptions are provided of the methane/air diffusion flame conditions, the characteristics of the SiCO fibers, the image acquisition and image analysis methods used, and the thermocouple measurements and radiative corrections. Finally some tradeoffs between SiCO fibers and thermocouples in terms of alignment and radiative corrections are presented.

2.1 Flame Description

The test flame was a coflowing methane-air laminar jet diffusion flame with a luminosity length of 72 mm burning at atmospheric pressure. Methane (99.99% purity) flowed upward through a 14 mm round port at 4.3 mg/s. Air flowed upward through a ceramic honeycomb and out of a 100 mm round coflow port at 1.7 g/s. Air came from a shop-air supply and was passed through a 0.3 μm oil filter and a 0.01 μm coalescing filter to remove oil, oil vapor and particulates. The fuel port extends 2 mm past the plane of the coflow port. Needle valves and pressure regulators were used to control the flowrates of air and methane. These flowrates were measured and monitored with rotameters. The rotameters were calibrated using soap bubble meters. The burner and the rotameters were leveled. The flame was sufficiently stable that no chimney or screen was needed.

Figures 2.1 and 2.2 show the basic elements of the experimental hardware. Visible in Fig. 2.1 are the burner and its fuel and air ports, the flame, two horizontal and glowing fibers, the fiber frame, the rotameters, the camera, and the black background. Fig. 2.2 shows a different view, where the fibers and their frame have
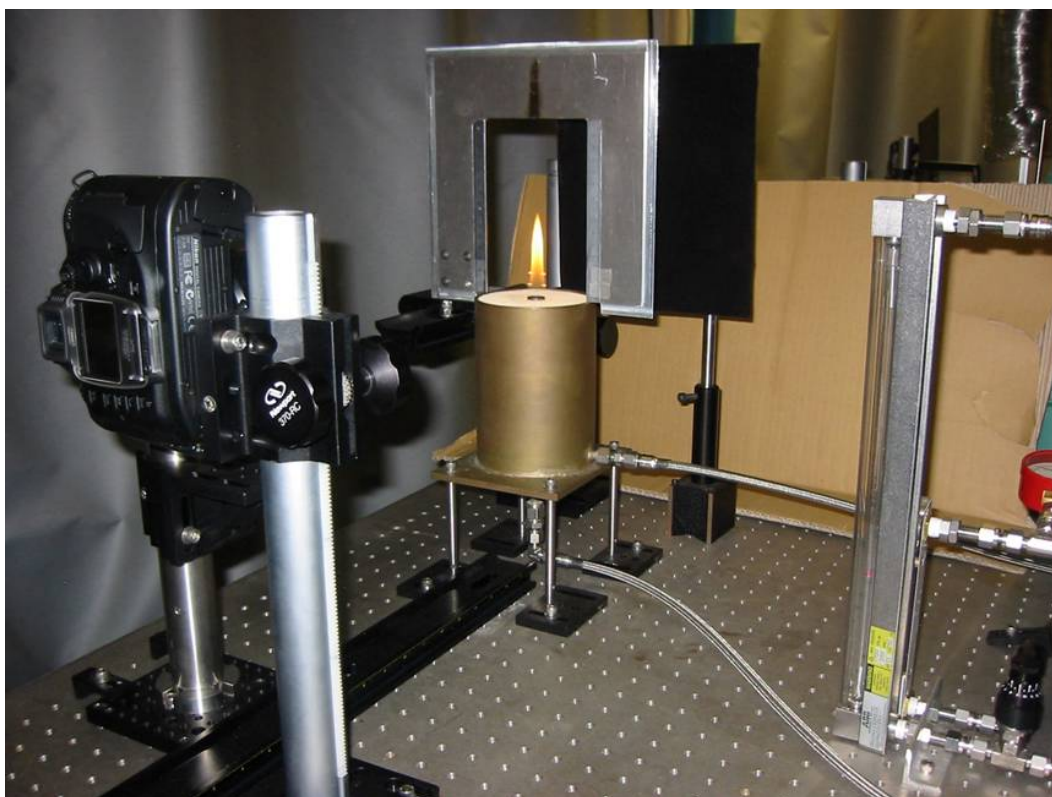
Fig. 2.1 Color image of experimental setup, view 1. The scale is indicated by the 72 mm flame.

been retracted. The air and methane rotameters are on the left and right, respectively. The blue Schott filter is visible in front of the camera here. Figure 2.3 is a dimensioned schematic of the setup (drawn to scale) which includes the burner and flame dimensions.

2.2 Fibers and Microscopy

The present SiCO fibers were cylindrical and approximately 14 μm in diameter. These fibers were manufactured by Nippon Carbon Co. and distributed by Dow Corning under the name Nicalon. Properties of the fibers, provided by the manufacturer, are given in Table 2.1 [22]. The fibers contain ultra-fine β-SiC crystals and an amorphous mixture of silicon, carbon and oxygen. The overall mass fractions of silicon, carbon and oxygen are 0.57, 0.32 and 0.12, respectively.
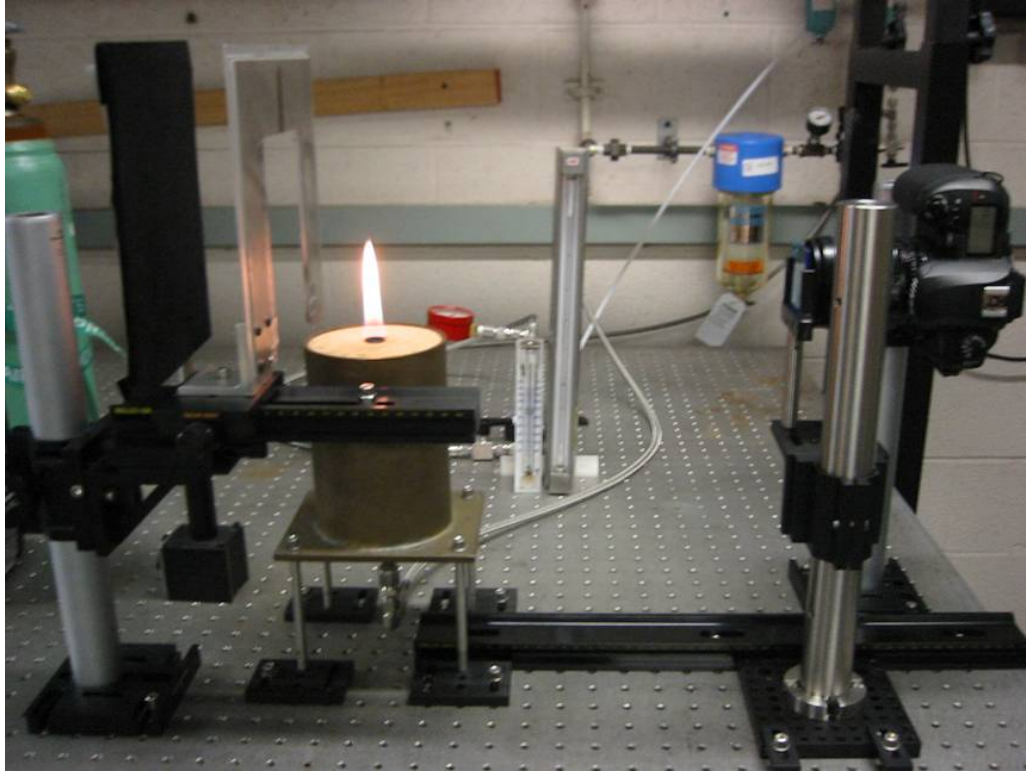
Fig. 2.2 Color image of experimental setup, view 2.
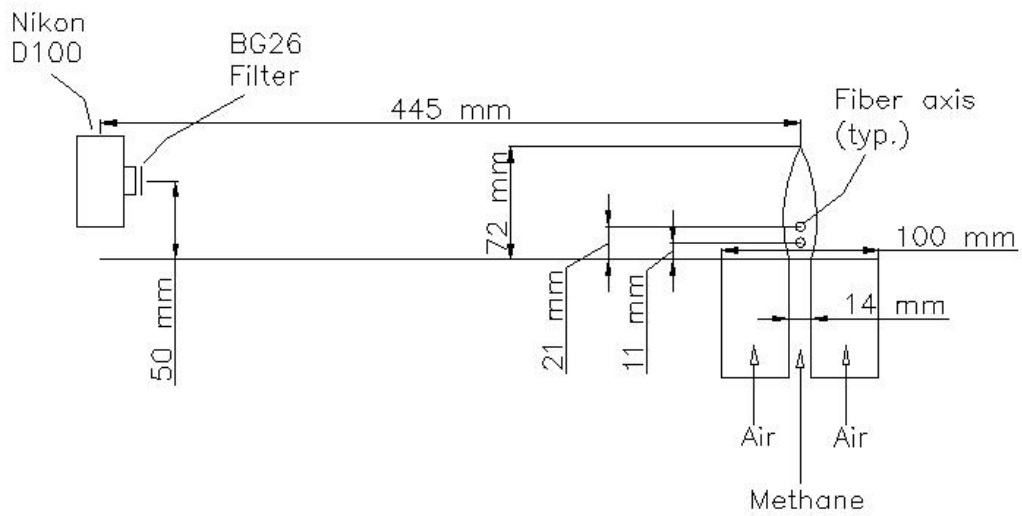
Fig. 2.3 Schematic diagram (drawn to scale) of experimental setup.

TABLE 2.1

Properties of NICALON™ Ceramic Grade SiCO fibers [102]

Property	Value
Fiber Denier	1800
Density, kg/m^3	2550
Composition, weight % Si:C:O	57:32:12
Filament Diameter, μm	14
Tensile Strength, GPa	3.0
Tensile Modulus, GPa	210
Vol. Resistivity, Ω-cm	1000
Dielectric Constant	9.2
Loss factor	1
CTE, ppm/ °C, 0-900 °C	3.9
Thermal Conductivity, W/m-K	
at 25 °C	2.97
at 500 °C	2.20
Specific Heat, J/g-K	
at 25 °C	0.71
at 500 °C	1.17
Surface Treatment	Polyvinyl Alcohol

The fibers are used most commonly in fabrics and composite materials. They were coated by the manufacturer with Polyvinyl Alcohol (PVA) to improve handling characteristics for manufacture. The fibers were provided on a spool as bundled yarn with a diameter of about 1 mm. The yarn was readily unraveled to provide the single-strand fibers used here.

Fibers 120 mm long were held by a frame and were stretched horizontally across the flame, as seen in Fig. 2.1. To prevent fiber sagging and motion, sufficient tension was applied to the fibers. The frame was attached to a translation stage to facilitate alignment and to allow the fibers to be heated in hot lean flame regions prior

to each test. This heating ensured the removal of residual PVA and soot particles deposited on the fibers.

Scanning electron microscopy (SEM) was performed with an ElectroScan E3-ORI-103 microscope. SEM was used here to obtain surface images of representative SiCO fibers and to measure fiber diameters. SEM provides high-resolution images of the surfaces of small objects but does not provide information about internal structures.

2.3 Image Acquisition

The flame and fibers were imaged with a Nikon D100 single-lens reflex color digital still camera. The camera contains a rectangular CCD of 23.7 × 15.6 mm with 3008 × 2000 pixels (6 megapixels). This is a consumer-grade camera. It is no longer produced by Nikon, but has been replaced with the Nikon D70, whose specifications are nearly identical. The current price of the Nikon D70 is US $500, which is unusually low for a camera that can be used for quantitative scientific imagery. This feature helped motivate Connelly et al. [21] to use a D70 for soot pyrometry in flames.

The various pixels of the Nikon D100 are sensitive to red, green or blue. The relationship among numbers of red, green, and blue pixels is approximately 1:2:1. The camera's interpolation yields 12-bit red-green-blue (RGB) intensities at each pixel. This bit depth provides RGB intensities in the range of $0 - 4095$. For the present tests, a monochrome camera would have been preferable but would have cost about ten times as much as the D100. The fill factor of the Nikon D100 sensor is not specified by the manufacturer but is less than 100%. Fill factor is the size of the CCD

8

light-sensitive area divided by the total CCD area. This non-unity fill factor could be problematic in the quantitative imaging of small objects like the fibers used here, but the tests that follow indicate that fill factor was not a limiting factor here.

Camera exposures were selected such that the fiber images were bright but did not saturate at any pixel in any color plane. Table 2.2 summarizes the camera settings used here. A Nikon 60 mm f/2.8 AF lens was used at f/3.3 and was focused on the flame axis. The International Standards Organization (ISO) film speed was set at 200. Automatic camera settings were avoided wherever possible, including those associated with focus, aperture, shutter speed, ISO, exposure compensation, tone, hue, white balance, image sharpening and noise reduction. A black background was used behind the flame (see Fig. 2.1).

The alignment and positioning of the camera is detailed in Fig. 2.3. The CCD plane was vertical and was 445 mm from the flame axis. The optical axis was 50 mm above the burner port. This configuration resulted in a spatial resolution in the object plane of 42 μm/pixel.

TABLE 2.2

Conditions for the present images[*]

Image	Fiber	Blue Filter	White Balance	Shutter Time, ms
1	unaged	no	direct sunlight	8
2	unaged	yes	incandescent	0.66
3	unaged	yes	incandescent	0.66
4	aged	yes	incandescent	0.66
5	none	yes	incandescent	0.66
6	unaged	yes	incandescent	100

* All exposures used ISO 200 and f/3.3

Initial images of glowing fibers revealed red and green intensities were far greater than blue intensities. This involved reduced signal-to-noise ratios at all blue pixels, which account for approximately 25% of the pixels. Two changes were introduced to improve the balance among the RGB intensities. Addition of a 3 mm thick 50 × 50 mm Schott BG 26 blue filter in front of the lens (with an increased shutter time) helped to equalize these intensities. The transmittances of red, blue and green wavelengths through the BG 26 blue filter are 22%, 90% and 86%, respectively. A white balance of incandescent with a color temperature of 2700 K also was introduced (using the Nikon menus) because this increased blue intensities by about 25%.

Images were recorded in Adobe RGB color space. Images were saved in uncompressed 12-bit Nikon Electronic Image Format (nef). They were then converted to tagged image file (tif) format using Nikon Capture Editor software (V3.5). The tif images were 12-bit images in 16-bit file formats. The nef and tif images required about 10 MB and 35 MB of data storage, respectively. Both formats contain the highest quality images available from the Nikon D100. The nef images require less data storage owing to their lossless compression algorithms.

2.4 Image Analysis

The recorded tif digital images were analyzed using the Spotlight 16 (V2004.8.27) software of Klimek and Wright [23]. This software is provided free by NASA and includes a convenient graphical user interface.

RGB intensities along selected lines were extracted from the tif images using Spotlight 16. These lines were either along or perpendicular to glowing fibers. The

lines were selected graphically using the Line Profile tool. For each pixel along the line, this tool plots and exports to a data file the x and y pixel coordinates and the RGB intensities (as 12-bit values) at that location. The Line Profile tool allows RBG intensities to be averaged across a selected line width (chosen between 1 – 5 pixels wide here).

The output from Spotlight 16 was arrays of x, y, R, G, B values. The x and y pixel coordinates were converted to height above burner and radius, where the origin is the center of the fuel port. This conversion was based on an image of a ruler aligned on the flame centerline. For some analyses the RGB intensities were converted to grayscales, which were defined as the average of the red, green and blue intensities.

Image subtraction of a flame-plus-fiber image minus a flame-only image also was performed in Spotlight 16. In this operation, subtraction was performed on the RBG intensities at corresponding pixels of the two images to yield a third tif image. Where subtraction resulted in negative intensities, Spotlight 16 assigned intensities of zero.

2.5 Thermocouple Measurements

Gas-phase temperatures (T_{gas}) were measured with an uncoated B-type thermocouple (Pt – 30% Rh versus Pt – 6% Rh) with a wire diameter of 51 μm and a butt-welded junction of the same diameter [24]. The thermocouple supports were 20 mm apart to minimize disturbances. The thermocouple was positioned horizontally with the flame axis closer to the junction than to any other part of the probe. Thermocouple temperatures (T_{TC}) were averaged over 60 s except at the flame sheet,

where peak instantaneous temperature was recorded. Thermocouple measurements were not recorded in regions where soot deposited, a condition that was recognized from temperatures that decreased with time.

Heat conduction along the thermocouple and fibers is a potential concern. A quantitative analysis of the errors due to conduction was performed. Experimentally, conduction was minimized in the thermocouple by aligning it perpendicular to the temperature gradient. Use of this alignment with the fibers would not allow TFP measurements along radial profiles in the flame and thus would severely restrict the region where temperatures could be measured with a single TFP image. Therefore for this work the fibers were oriented along horizontal lines through the flame centerline. As shown below, the significantly reduced diameter and thermal conductivity of the fibers, relative to those of the thermocouple, minimize conductive errors despite this alignment choice.

In the quantitative analysis, the thermocouple temperature and surroundings were assumed to be steady. The thermocouple was assumed to radiate as a cylindrical graybody with an emissivity of 0.2 [25]. This assumes no soot deposit occurs on the thermocouple. With soot deposition emissivity can be expected to be as high as unity. The thermocouple is steadily heated by convection and cooled by radiation and conduction according to:

$$h\,(\,T_{gas} - T_s\,) = \sigma\ \varepsilon\,(\,T_s^{\,4} - T_\infty^{\,4}\,) - (\,k_s\,d\,/\,4\,)\ \mathrm{d}^2 T_s\,/\,\mathrm{d}x^2 \qquad (2.1)$$

Thermal conductivity of the SiCO fiber is 2.20 W/m-K (Table 2.1) and that of the thermocouple is 69.87 W/m-K [26]. The $\mathrm{d}^2 T_s\,/\,\mathrm{d}x^2$ for the thermocouple and the fiber were estimated from the thermocouple measurements. For the present fibers, Eq. (2.1)

indicates that radiative corrections are 320 times greater than those for conduction at the peak temperature, in agreement with Ref. [1], and thus are neglected below. The product of thermal conductivity and the diameter of the cylindrical probe appear in the conduction error term, indicating that conduction errors are worse for thermocouples than for fibers. For a thermocouple oriented radially, radiation rate divided by conduction rate is 0.61. Thus to avoid conduction errors the thermocouple was oriented perpendicular to the temperature gradient.

A determination of the convection heat transfer coefficient, h, now allows T_{gas} to be determined from Eq. (2.1). This coefficient is calculated here assuming nitrogen gas flows past the thermocouple at 1 m/s. Convective heat transfer coefficient was measured and correlated by Nakai and Okazaki [27] for small cylinders in crossflow with $Pe < 0.2$ as:

$$Nu = [\, 0.8237 - 0.5 \, ln \, (\, Pe \,) \,]^{-1} \tag{2.2}$$

where the dimensionless numbers are defined as:

$$Nu = h \, d \, / \, k_{gas} \tag{2.3}$$

$$Pe = Re \, Pr = V \, d \, / \, \alpha \tag{2.4}$$

and a Prandtl number of 0.7 is assumed.

Reynolds number depends on viscosity, which was obtained here from Mills [28] for nitrogen at 1.01 bar:

$$v(T) = 6.2834\text{e-}11 \; T^2 + 5.9794\text{e-}8 \; T + 7.6259\text{e-}6 \tag{2.5}$$

where v is in m^2/s and T is in K. Gas thermal conductivity k_{gas} is a function of temperature and is correlated for nitrogen at 1.01 bar in the CRC handbook [29] as:

$$k_{gas}(T) = 5.107\text{e-}5 \; T + 0.01141 \tag{2.6}$$

K_{gas} has the units W/m-K.

Transport properties correspond to nitrogen at the average of the probe and gas temperatures. Velocity was estimated at 1 m/s based on velocity measurements near the flame sheet in similar flames [30,31].

Equations (2.1 – 2.4) can be combined to yield the following relationship for the radiative temperature correction

$$T_{gas} - T_s = \sigma \varepsilon d (T_s^4 - T_\infty^4) [0.8237 - 0.5 \, ln (V d / \alpha)] / k_{gas} \qquad (2.7)$$

The transient response of a cylindrical probe (fiber or thermocouple) in a crossflow was also calculated. This is expressed as an overall energy balance on the solid. The rate of change of sensible heat of the probe equals the rate of heat transfer at the surface as shown in Eq. (2.8). This equation neglects the contribution from the radiative heat transfer:

$$m \, c_p \, dT_s / dt + h \, A(T_s - T_\infty) = 0 \qquad (2.8)$$

Integration of Eq. (2.8) yields the time constant of the cylinder as

$$\tau = \rho_s d^2 c_p / 4 \, Nu \, k_{gas} \approx \rho_s d^2 c_p / 1.6 \, k_{gas} \qquad (2.9)$$

where the approximate relation here assumes a typical Nu of 0.4 for these probes in this flame. For the thermocouple in the present study, $\rho_s = 2.145e7$ g/m^3 and $c_p = 154$ J/kg-K, this yields a time response of 64 ms. The transient time response of the fiber is 4.3 ms, in agreement with Ref. [1], indicating a faster temporal response than the thermocouple. The related properties of the SiCO fiber are given in Table. 2.1.

2.6 SiCO Fiber Radiation Corrections

The radiative correction methodology applied to the thermocouple temperature measurements was also applied to the SiCO fibers. Gas temperatures, determined

from Eq. (2.7), were used to estimate the temperatures ($T_{fiber,est}$) along a horizontal radiating SiCO fiber at the same positions. The radiative/convective balance was conducted similarly to that for the thermocouple, using a fiber diameter of 13.9 μm and a fiber emissivity of 0.88 [3,8,9,15].

The radiative correction of Eq. (2.7) is proportional to emissivity times diameter (with diameter also having a small contribution in the logarithm term). This product is 10.2 μm for the present thermocouple and 12.2 μm for the SiCO fibers. Thus it is anticipated that the radiative correction for the fibers will be about 20% higher than those for the thermocouple.

2.7 Uncertainty Analysis

Thermocouple temperatures had an estimated uncertainty of ± 20 K arising from flame motion and voltage measurements. The thermocouple T_{gas} measurements have estimated uncertainties that increase with T_{gas}, are up to ± 40 K, and arise from uncertainties in T_{TC}, local velocity, and Eq. (2.2). Uncertainties in $T_{fiber,est}$ are estimated at up to ± 30 K. This is lower than uncertainties in T_{gas} because of the way radiation corrections were first added and then subtracted. The scatter in the TFP measurements (as seen in a later figure) is about ± 20 K.

Chapter 3: Results and Discussion

The results of the TFP technique are presented here. Representative fibers were examined in the SEM. Color images of the flame and glowing fibers are presented. The thermocouple measurements are shown. Finally results of the TFP calibration and measurements are given.

3.1 Fiber Microscopy

Accurate TFP requires fibers with uniform diameter and surface composition. To address this, representative SiCO fibers were examined by SEM. Figure 3.1 shows an SEM image of a typical untreated sample SiCO fiber. The fiber in Fig. 3.1 has the appearance of a smooth cylindrical object to which an irregular coating has been added. This coating is believed to be the PVA sizing used by the manufacturer to improve the fiber handling characteristics.
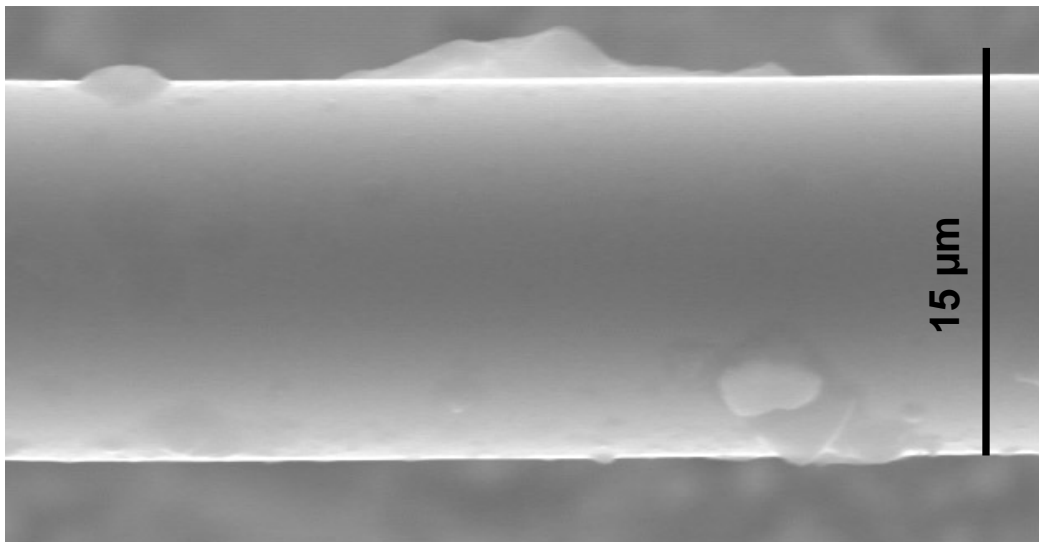
Fig. 3.1 Grayscale SEM image of a typical untreated SiCO fiber.

It was found that sizing was easily removed by treating fibers (heating them to glowing) in fuel-lean regions of the methane/air flame. An SEM image of a typical treated SiCO fiber is shown in Fig. 3.2. This image shows that this treating process yields fibers whose surfaces are smooth and uniform. Mean diameters of treated fibers were measured and were found to be 13.9 μm (in agreement with the manufacturer's value of 14 μm, see Table 2.1), with a standard deviation of 0.19 μm. The excellent uniformity in diameter and surface appearance suggests these treated fibers are well suited to TFP.

Although the present fibers contain 12% (by mass) oxygen, they are not fully oxidized and are subject to further oxidation (called aging here) when placed in hot lean flame regions. After approximately 60 minutes in the present flame, fibers were found to begin to change from black to grey. The effects of moderate aging on TFP were considered here. Unaged fibers were held in the test flame for about 10 minutes to age them. Examination of these fibers in the SEM did not reveal any differences in
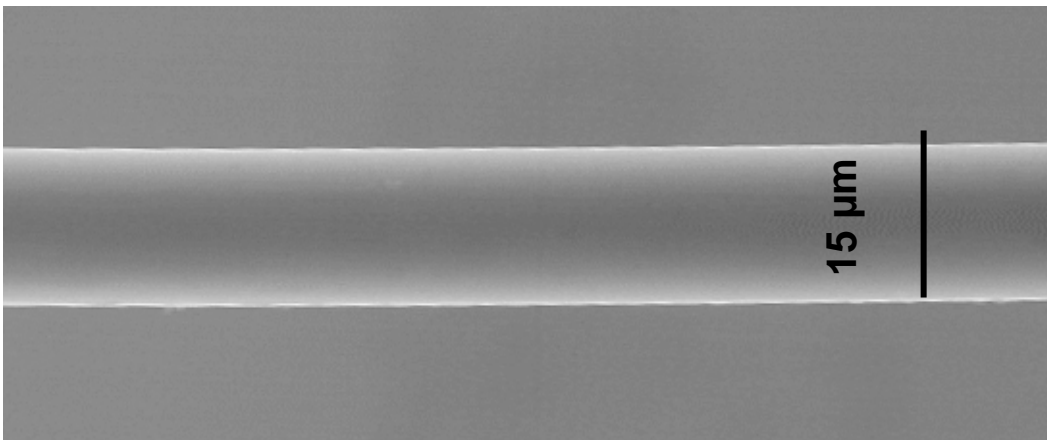

Fig. 3.2 Grayscale SEM image of a typical treated SiCO fiber. This fiber was treated by holding it in a hot lean region of the test flame.

the surface appearance suggesting that TFP measurements are not affected by moderate aging of the fiber.

3.2 Flame Images

A color image of the test flame with glowing fibers is shown in Fig. 3.3. This image was recorded with the same camera as used for TFP, but here the blue Schott filter was removed and a white balance of direct sunlight was used. The test flame is attached to the burner and has a luminosity length of 72 mm. Yellow emissions from soot first appear near the flame sheet at a height of 9 mm. The effects of soot luminosity are discussed below. The flame was nearly steady but wavered slightly from side to side, especially at higher axial locations. This wavering introduced minor difficulties in aligning the TC and TFP results.
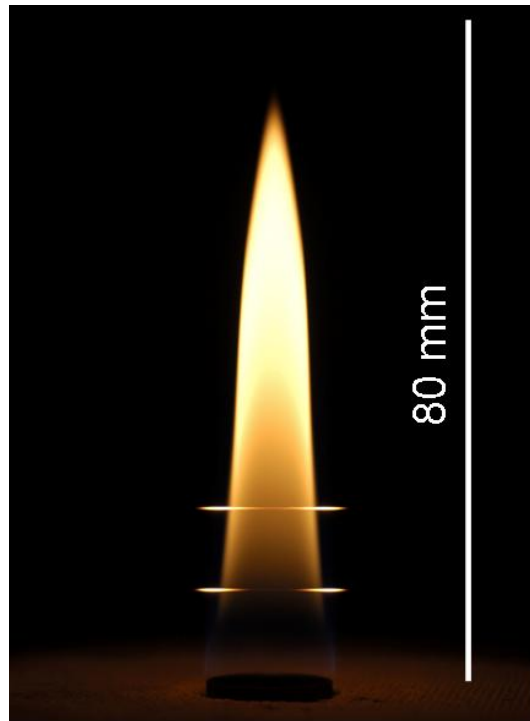

Fig. 3.3 Color image of the co-flowing methane-air laminar jet diffusion flame with fibers at heights of 11 and 21 mm. This is Image 1 of Table 2.2.

Horizontal fibers at heights of 11 and 21 mm are seen glowing in this image. These heights were chosen because they allow TFP to be examined at 11 mm with almost no soot and at 21 mm where more soot is present. They were moved into position about 2 s before this image was recorded to minimize soot deposition on the higher fiber. Despite flame and soot luminosity, the fibers are brighter than their surroundings.

Figure 3.4 shows three color images that were used in the present TFP analysis. These images have been cropped from the original size of 3008 × 2000 pixels. Figure 3.4(a) is an image of the test flame with fibers. To ensure that the fibers in Fig. 3.4(a) were bright but did not saturate in any color plane, settings included an ISO of 200, a shutter time of 0.66 ms, and f/3.3 (see Table 2.2).

Flame and soot luminosity can interfere with TFP. Figure 3.4(a) shows flame luminosity was negligible at 11 mm height but not at 21 mm. To reduce the effects
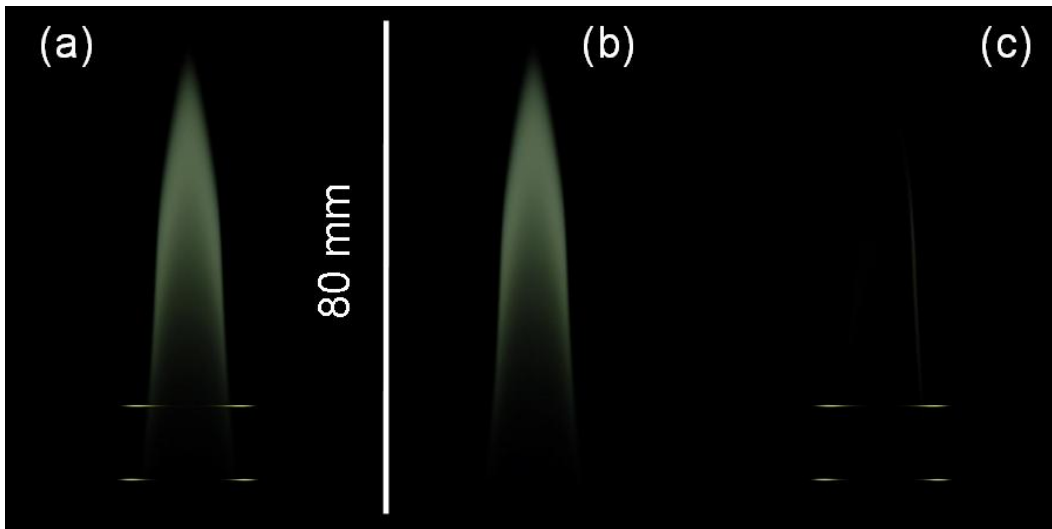

Fig. 3.4 Color images of one image sequence used in TFP analysis.
a) Flame and fiber. (Image 2 of Table 2.2)
b) Flame only. (Image 5 of Table 2.2)
c) Flame background subtraction (Image (2) minus Image (5)).

of flame luminosity at 21 mm, a separate image was recorded, without fibers, shown in Fig. 3.4(b). Subtraction of Fig. 3.4(b) from Fig. 3.4(a) resulted in an image of the fibers alone, as shown in Fig. 3.4(c). Negative intensities that arose from this subtraction were assigned zero values. Subtractions of this type will introduce measurement errors unless the CCD sensitivity is linear. The results that follow indicate any such errors are small here. Background subtraction had a negligible effect for the fiber at 11 mm and thus was used only at 21 mm.

3.3 Thermocouple Measurements

Fiber and thermocouple temperatures as a function of gas temperature for steady conditions are shown in Fig. 3.5. This plot assumes nitrogen gas at 1 bar flowing at 1 m/s and is defined by Eq. (2.7) and the associated discussion. Thermocouples and fibers generally do not record actual gas temperatures. Both types of probes have lower temperatures than the local gas temperature owing to radiative losses.

Figure 3.5 indicates that radiative corrections increase with temperature. This is supported by the fourth power of probe temperature that appears in Eq. (2.7). The plot also shows that the radiative correction is larger here for the fibers than for the thermocouple. As discussed in Section 2.6, this arises from the product of graybody emissivity times probe diameter that appears in Eq. (2.7).

Profiles of the measured gas, thermocouple and fiber temperatures at a height of 11 mm are shown in Fig. 3.6. The raw thermocouple measurements are shown as solid triangles. These measurements were converted to the estimated gas and fiber temperatures in Fig. 3.6 using Eq. (2.7), or, equivalently, Fig. 3.5.
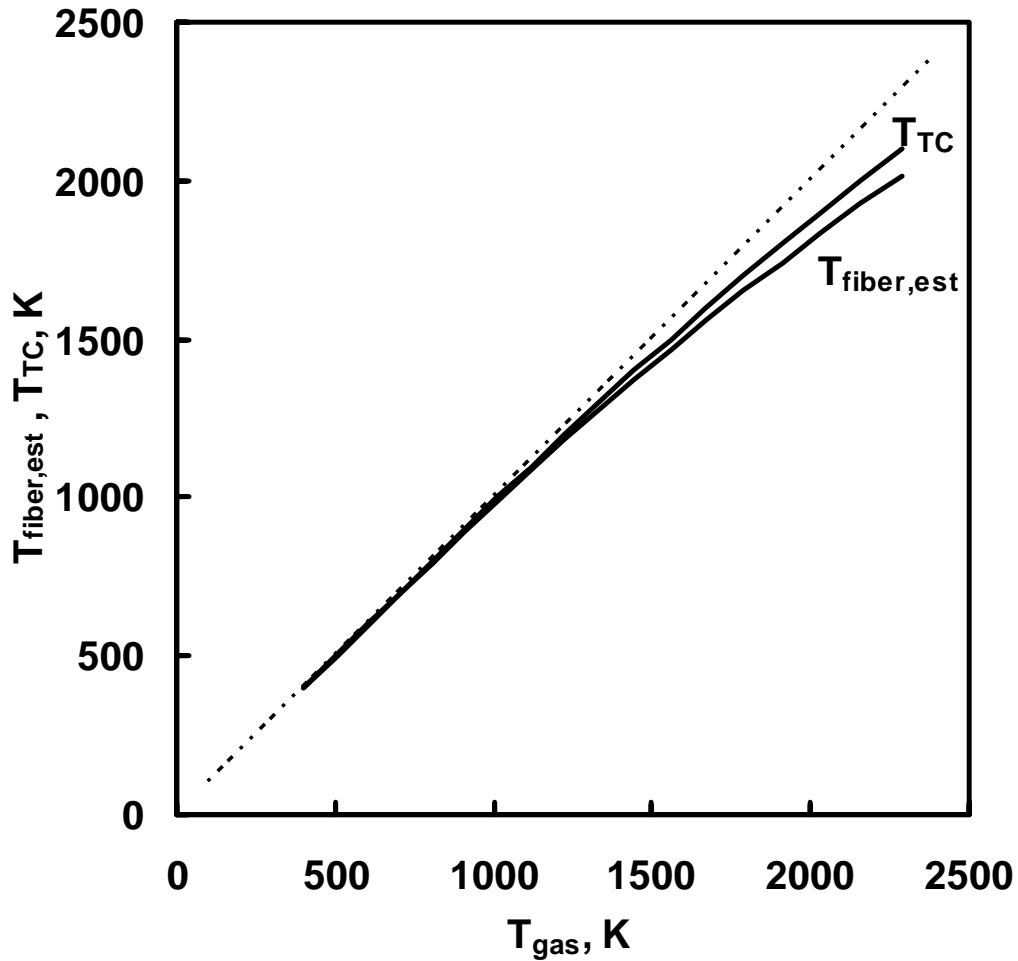
20

Fig. 3.5 Fiber and thermocouple temperatures as a function of gas temperature. Equations are $T_{fiber,est} = -3.17853\text{E-}5\ T_{TC}^2 + 1.031\ T_{TC} - 9.42002$ and $T_{gas} = 8.82611\text{E-}5\ T_{TC}^2 + 0.88134\ T_{TC} + 40.0929$ with all temperatures in Kelvin.

A sharp temperature peak is evident at the flame sheet at a raduis of 7 mm. At radii greater than 9 mm all three temperature profiles converge because of smaller radiation corrections at lower temperature. At the peak T_{TC} of 2024 K, the gas is 162 K hotter than the thermocouple and 238 K hotter than the fiber. The highest T_{gas} observed is 2186 K, which is reasonable given the adiabatic flame temperature of methane/air mixtures of 2223 K [32].

Similar measured temperature profiles, here at a height of 21 mm, are shown in Fig. 3.7. Fewer measurements are reported here because at this height soot deposition
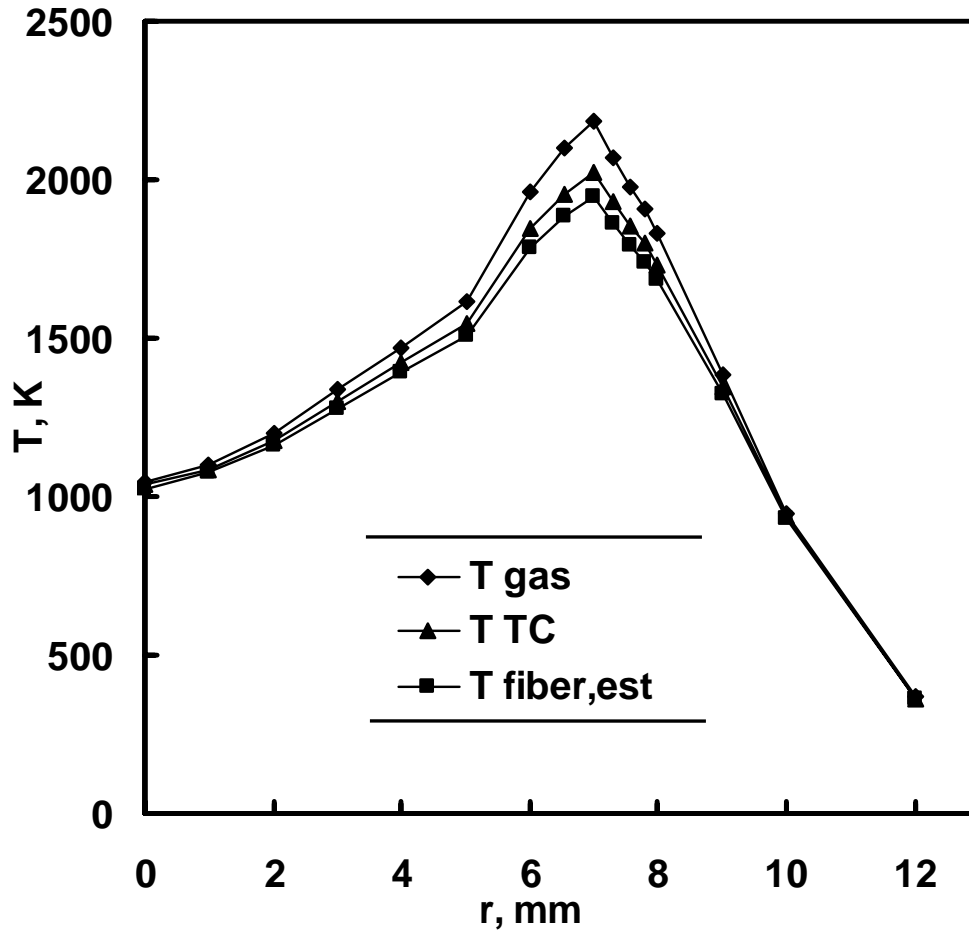
Fig. 3.6 Measured gas, thermocouple and fiber temperatures at a height of 11 mm.

on the thermocouple occurred for locations within 5 mm of the flame axis. This was detected by temperature readings that decreased with time. The peak gas temperature at this height is 2170 K, reflecting radiative losses from soot and carbon dioxide.

Figures 3.6 and 3.7 show temperature measurements only along one radial line at each height. Additional thermocouple measurements indicated that the results were repeatable along other radial lines and that the flame was axially symmetric, as the image of Fig. 3.3 suggests.
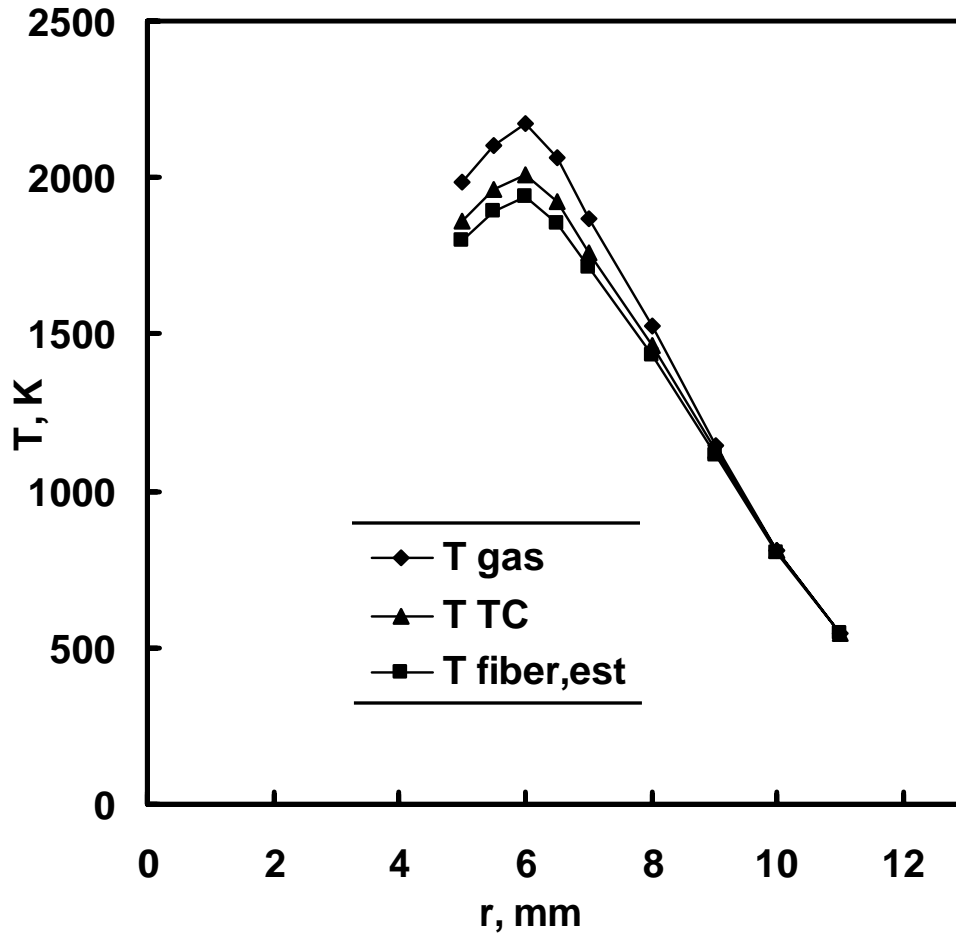
Fig. 3.7 Measured gas, thermocouple and fiber temperatures at a height of 21 mm.

3.4 TFP Calibration

The present TFP diagnostic was calibrated using the radiation-corrected thermocouple measurements at 11 and 21 mm heights. Fiber intensities at these heights were obtained from line profiles along the SiCO fibers.

TFP signal-to-noise ratios can be compromised by line profiles along fibers that are either too narrow or too wide. The width of the line profiles was chosen based on the full-width-half-maximum (FWHM) dimensions of the fiber images. To find the FWHM dimensions, single-pixel-wide fiber intensity profiles normal to glowing fibers were considered. Typical results are shown in Fig. 3.8. At the peak fiber

temperature (1940 K), the imaged glowing fibers had widths of 4.9 pixels FWHM. At a lower fiber temperature of 1530 K the fibers had widths of 3.7 pixels FWHM. Reflecting these observations, line profiles with 5 pixels FWHM were used throughout in the TFP results that follow.

The increased imaged fiber width upon heating of Fig. 3.8 has been reported before [18] and is evident to the naked eye. This phenomenon remains unexplained and warrants further study. Note that a FWHM width of 5 pixels corresponds to a width of 210 μm in the object plane despite fiber widths of 13.9 μm.

Figure 3.9 shows profiles of fiber temperature and the red, green and blue fiber intensities for an unaged fiber at 11 mm height. The fiber temperatures are
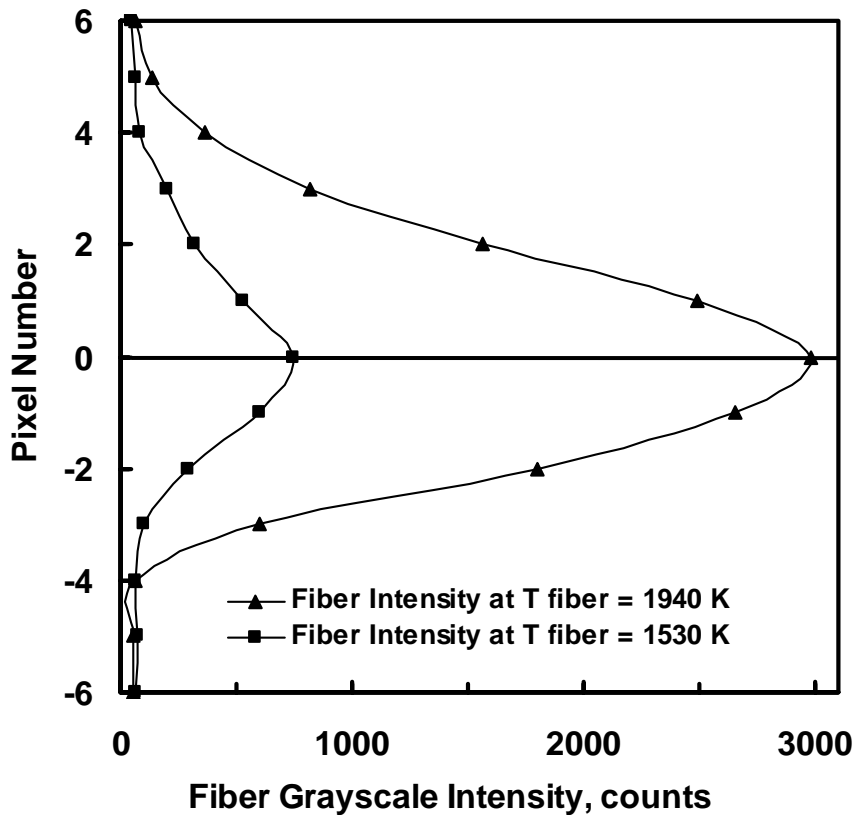

Fig. 3.8 Fiber intensity profile normal to fiber at fiber temperatures of 1940 K and 1530 K at a height of 11 mm. These profiles are one pixel wide.

reproduced here from Fig. 3.6. These fiber intensities come from a single image, Image 2 of Table 2.2. A line profile (five pixels wide) was extracted from Image 2 using Spotlight 16. This profile crossed the flame sheet twice (once each for the left and right sides as viewed by the camera), thus this fiber provided two realizations of intensity versus radius for each color, as shown in Fig. 3.9. The profiles were shifted slightly here to align with the thermocouple profiles in consideration of small flame motions.

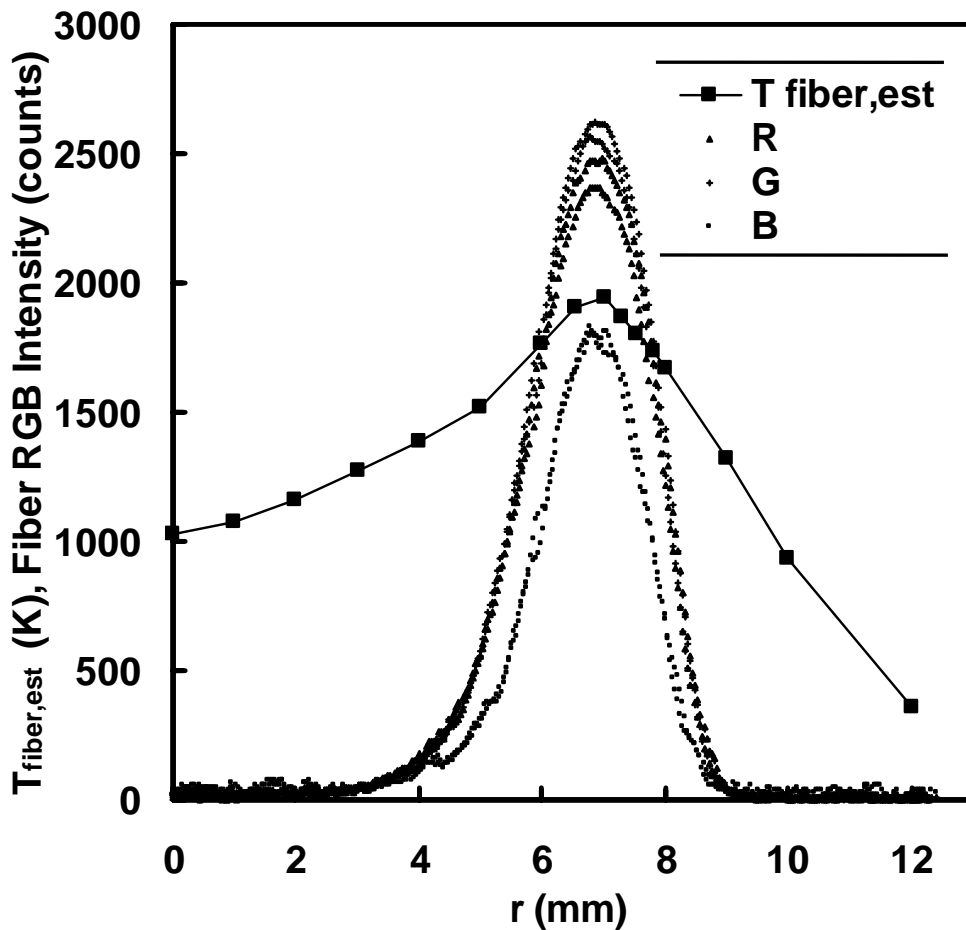Fig. 3.9 Fiber temperature (from Fig. 3.6) and fiber R,G,B intensities versus radius at 11 mm height. Flame background intensities have not been subtracted. The number of fiber intensity data shown for each color is 601 and these data come from Image 2.

The good agreement between the left- and right-side intensity realizations of Fig. 3.9 indicates the test flame is nearly perfectly axisymmetric. Despite the inclusion of the blue Schott filter and a custom white balance, the blue pixels remain dimmer than the red and green pixels. The data spacing here is 42 μm, corresponding to the spatial resolution of the pyrometer.

Figure 3.10 shows similarly obtained results, here at a height of 21 mm. Unlike Fig. 3.9, the fiber intensities here were obtained after image subtraction
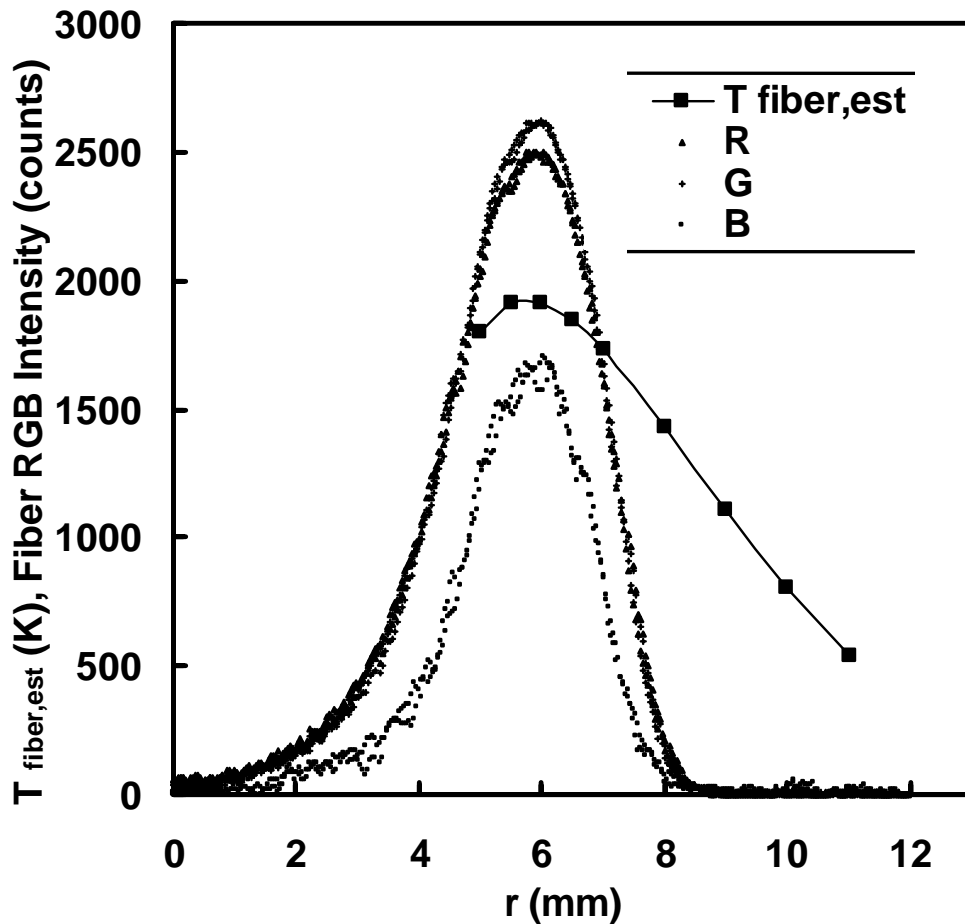

Fig. 3.10 Fiber temperature (from Fig. 3.7) and fiber R,G,B intensities versus radius at 21 mm height. Flame background intensities have been subtracted. The number of fiber intensity data shown for each color is 601 and these data come from Images 3 and 5.

(Image 3 minus Image 5). This was found to be helpful in minimizing the effects of flame luminosity near the fiber at this height. The peak fiber intensities for each of the red, green, and blue and colors were similar to those obtained at a height of 11 mm. The fiber intensity profiles are broader than at 11 mm, indicating reduced temperature gradients at 21 mm.

Note that filament intensities could be obtained at a height of 21 mm even within 4 mm of the flame axis, where thermocouple measurements were problematic owing to soot deposition. Although soot was found to deposit on the fibers at these locations, it did not significantly interfere with the TFP measurements. There are two reasons for this. First, soot deposition on thermocouples (but not on fibers) dramatically increases the surface emissivity and the resulting radiative corrections. Second, the present TFP measurements were performed with the fiber in the flame for as short as 2 s. In contrast, the thermocouple measurements were averaged over 60 s.

The RGB intensities of Figs. 3.9 and 3.10 were converted to grayscale intensities and plotted in Fig. 3.11. This figure also includes grayscale intensities from images of a second pair of unaged fibers (Image 3) and a pair of aged fibers (Image 4). As before, image subtraction was performed at 21 mm but not at 11 mm. At each height, images of three fibers provide realizations of six intensity profiles at each height in Fig. 3.11. Estimated fiber temperatures are again reproduced from Figs. 3.6 and 3.7. The conversion from RGB to grayscale reduces by two thirds the number of data points in plots of intensity versus location. However, such conversion is favored here because this type of averaging reduces scatter and it collapses the three color intensity profiles at each height into a single profile.
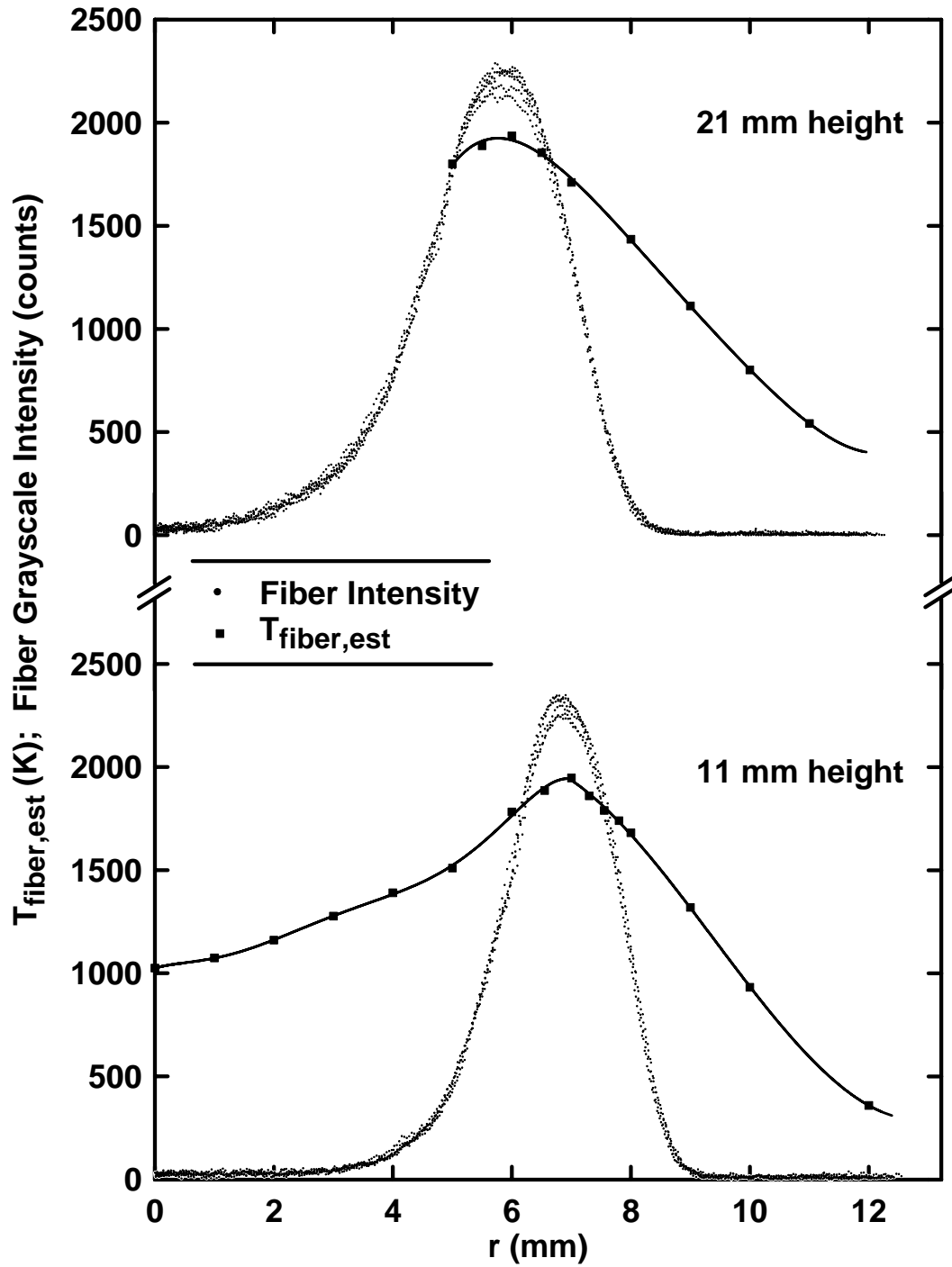
Fig. 3.11 Fiber temperature (from Figs. 3.6 and 3.7) and fiber intensities at heights of 11 and 21 mm. At each height $T_{fiber,est}$ is fit with one or two polynomials, one each to the left and right of the temperature peak. The number of fiber intensity data shown is 1803 at each height and come from Images 2, 3, 4 and 5.

The $T_{fiber,est}$ versus radius data of Fig. 3.11 were fitted with polynomials as shown. This allowed each intensity measurement to be associated with an estimated fiber temperature. The resulting correlation between fiber temperature and intensity is shown in Fig. 3.12, where both 11 and 21 mm heights are included. This is the TFP calibration plot. The correlation is good for $T_{fiber,est}$ in the range of $1350 - 1950$ K, with scatter in the TFP measurements of about ± 20 K.

Guidance is provided here for future investigators interested in calibrating a TFP system. The most reliable and accurate method would be to reproduce the steps detailed here. An alternate would be to use the same optics, camera, and camera settings as selected here, along with the calibration of Fig. 3.12. This may not possible if a different viewing configuration or temperature range is desired. Another option would be to recognize that the data of Fig. 3.12 is roughly linear at high temperatures. Thus, a two-point calibration may suffice. Finally, the data of Fig. 3.12 reveals a roughly linear relationship between temperature and grayscale intensity for temperatures above 1500 K. The best-fit line through this data has a slope of 0.215 K/grayscale. Using this slope it should be possible for future investigations to perform approximate TFP based on a single thermocouple measurement (or a single assumed temperature).

The calibration of Fig. 3.12 can also be performed individually for each of the RGB colors rather than for grayscales. As discussed above this increases by a factor of three the number of intensity data but introduces noise and different calibrations for each color. Figure 3.13 is a plot of $T_{fiber,est}$ versus RGB fiber intensity from Image 2 at a height of 11 mm. This plot was made from the $T_{fiber,est}$ versus radius data of
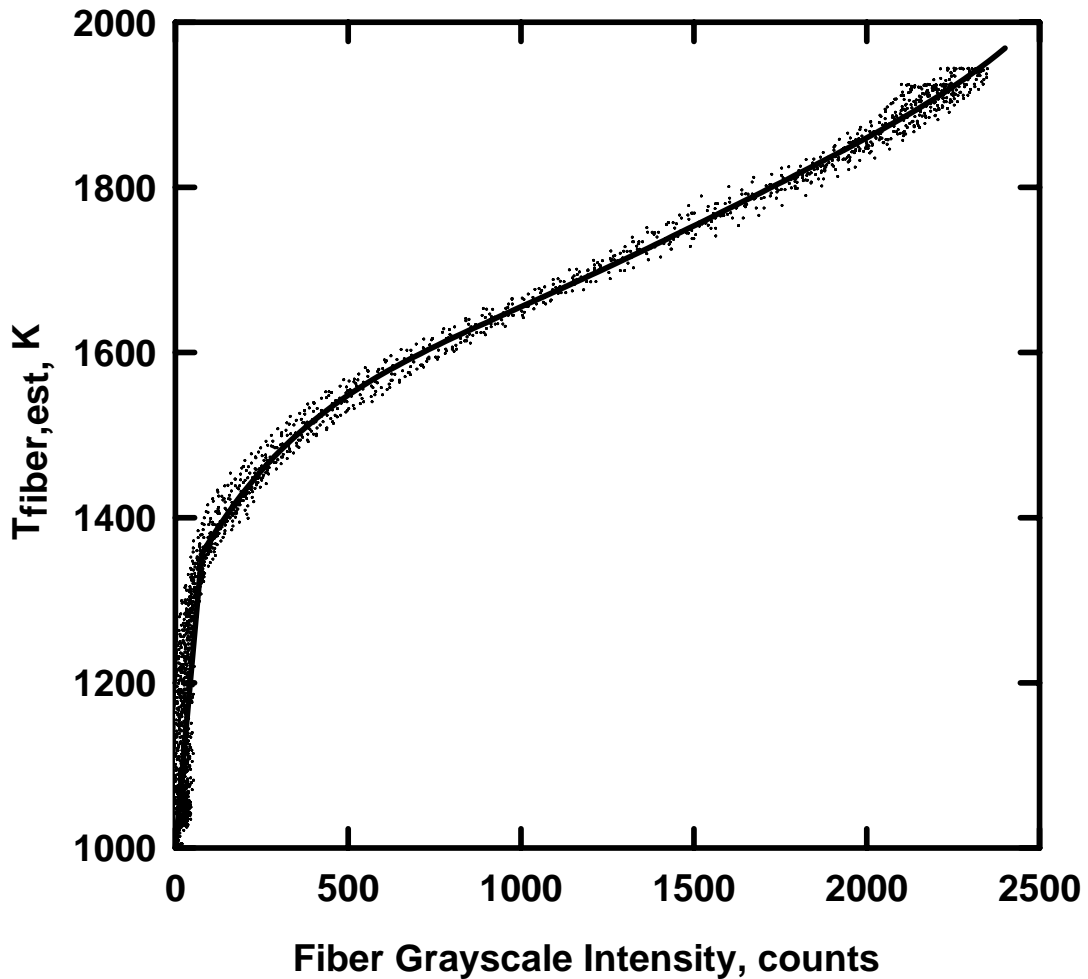
Fig. 3.12 Estimated fiber temperature versus intensity for temperatures above 1000 K at 11 and 21 mm heights. A total of 2072 data are plotted. The data fits shown are a line below 1350 K and a fifth-order polynomial above 1350 K. The equations are $T_{fiber,est} = 4.6667(GS) + 1000$ and $T_{fiber,est} = 3.54200833E\text{-}14(GS)^5 - 2.56195368E\text{-}10(GS)^4 + 7.28509888E\text{-}7(GS)^3 - 1.00053137E\text{-}3(GS)^2 + .851512406(GS) + 1296.65403$

Fig. 3.9 similarly to how the calibration of Fig. 3.12 was produced from the data of

Fig. 3.11. The corresponding RGB calibration at 21 mm is shown in Fig. 3.14. Figs.

3.13 and 3.14 are not essential to the present study but are included here for

completeness. They also are of interest to the possible development of a TFP

diagnostic that relates color (rather than intensity) to temperature. Such a system

Fig. 3.13 Fiber temperature versus fiber R,G,B intensities at 11 mm height. Flame background intensities have not been subtracted. The number of fiber intensity data shown for each color is 483 and this data comes from Image 2.

would be less affected by soot deposition on fibers, obscuration by smoke, and camera drift.

3.5 TFP Results

The data fits of Fig. 3.12 were used to convert each measured fiber intensity to fiber temperature. Radiation corrections (from Fig. 3.5) were then applied. This allowed plots of gas temperature derived from TFP versus radius, shown in Fig. 3.15.
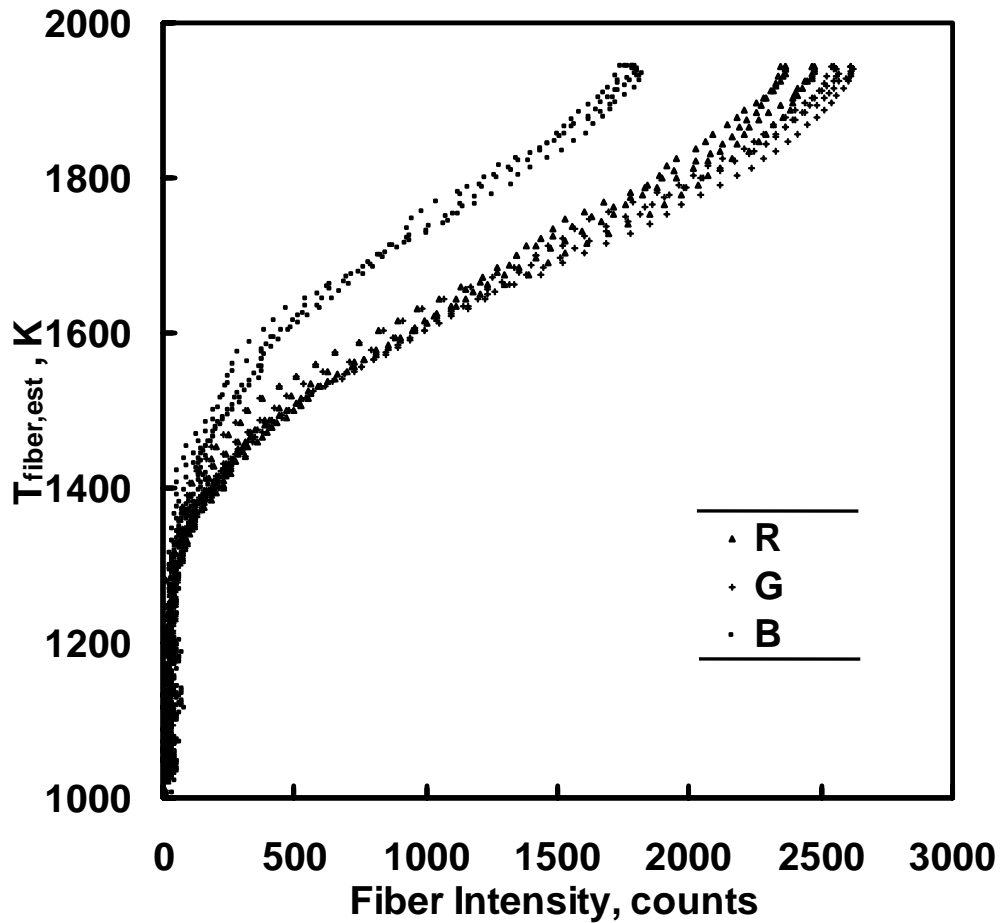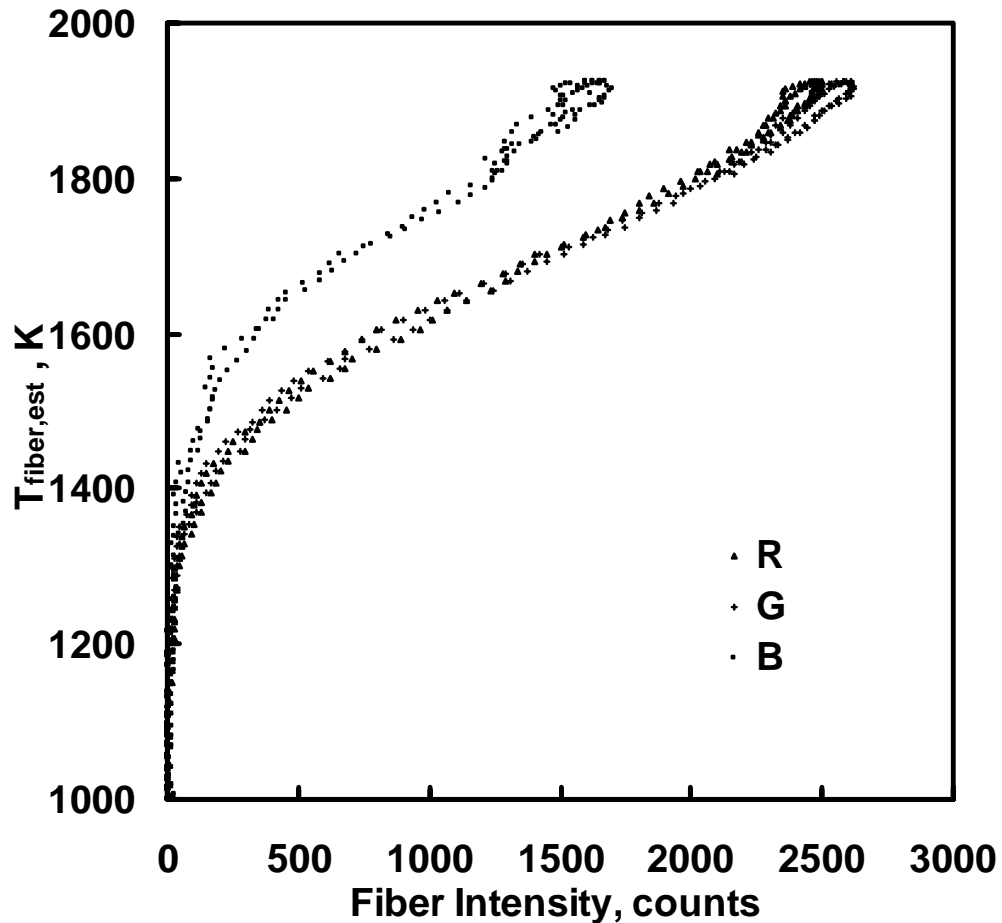
Fig. 3.14 Fiber temperature versus fiber R,G,B intensities at 21 mm height. Flame background intensities have been subtracted. The number of fiber intensity data shown for each color is 206 and this data comes from Images 3 and 5.

Also included are the thermocouple based gas temperatures of Figs. 3.6 and 3.7. Figure 3.15 shows that the TFP diagnostic yields reasonable gas temperatures in the range 1400 – 2200 K. In consideration of the scatter in this plot and estimated uncertainties in thermocouple gas temperatures, it is estimated that the uncertainty in the TFP gas temperatures is ± 60 K.

TFP scatter increases below gas temperatures of 1400 K owing to the camera's limited sensitivity range. Additional images at exposures of up to 0.1 s (see Table 2.2) indicate that gas temperatures as low as 800 K can be measured by the present

system. At longer exposures, however, saturation and data loss occur at the highest temperatures.

Figure 3.15 is a comparison of TFP and thermocouple measurements. Note that the TFP measurements were calibrated by the thermocouple measurements. This figure is included to indicate the capabilities of this TFP diagnostic. If the calibrated TFP system were applied to a different flame, the scatter and agreement with thermocouple data is expected to be similar to that of Fig. 3.15.

Data in Fig. 3.15 at 21 mm height illustrate how regions of light soot loading (at radii below 5 mm) allow temperature measurements by TFP where thermocouple measurements are problematic. Further increases in soot concentrations could also preclude TFP measurements owing to high rates of soot deposition and high background luminosity.

TFP has been demonstrated here for the first time using a consumer grade digital camera. This should bring this diagnostic within the budgetary restrictions of a large number of combustion researchers. In addition, the durability of this camera allows TFP to be performed in microgravity drop towers.
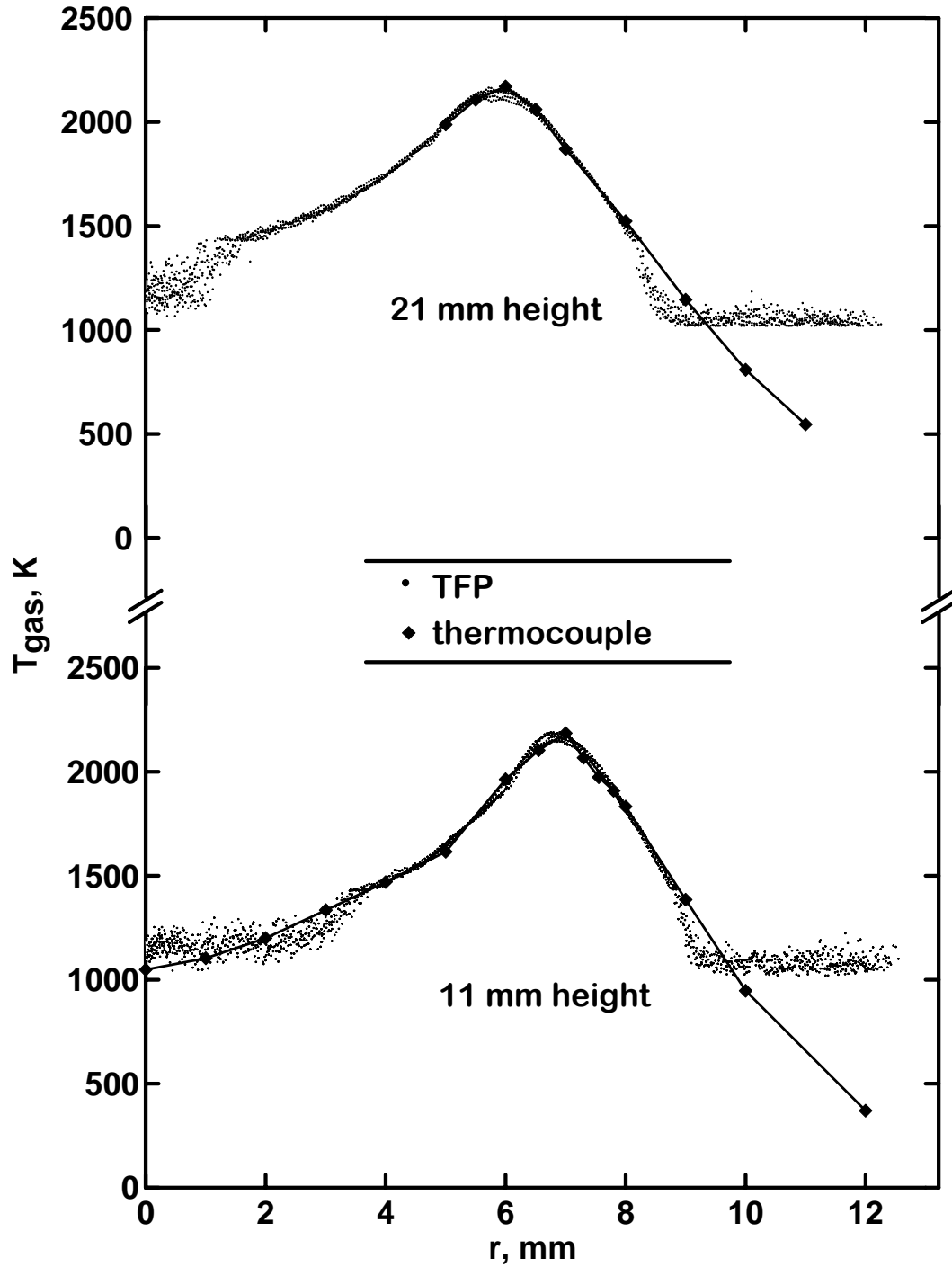
Fig 3.15 Gas temperature versus radius determined by thermocouple and TFP at heights of 11 and 21 mm. Thermocouple data are connected by straight lines. The number of fiber intensity data shown is 1803 at each height.

Chapter 4: Conclusions

Thin-filament pyrometry was conducted in a methane/air laminar diffusion flame using a digital still camera. Thermocouple measurements were performed to calibrate the TFP system. The major findings are:

(1) TFP has been demonstrated with an inexpensive digital color still camera. This camera has the highest pixel resolution (3008 × 2000) of any camera used to date for TFP. Its bit depth of 12 exceeds that of many previous cameras used for TFP. The low cost and high performance of this camera make it well suited for TFP. Its self-contained power supply and memory and its durability allow its use in microgravity drop towers.

(2) The TFP system yielded gas temperatures in the range of 1400 – 2200 K with an estimated uncertainty of ± 60 K, a relative temperature resolution of ± 0.215 K, a spatial resolution of 42 μm and a temporal resolution of 0.66 ms.

(3) For the present methane/air diffusion flames, the TFP method was able to measure temperatures in regions containing soot. These regions were problematic for thermocouple measurements because steady measurements were impossible and emissivity was unknown.

(4) Fiber intensity profiles normal to the fibers revealed that the fiber image width increased with increased fiber temperature. At fiber temperature of 1940 K and 1530 K the FWHM fiber width was 4.9 pixels and 3.7 pixels respectively.

(5) The present SiCO fibers were found by SEM to have a mean diameter of 13.9 μm with a standard deviation of 0.19 μm. Different fibers yielded identical intensities in the present flames within experimental uncertainties. Aging the fibers in a hot

flame zone for 600 s was found to have no effect on the appearance of the fibers in the SEM or on the TFP measurements.

The TFP system developed here can be used affordably in other laboratories. For the highest accuracy, full calibrations like the one herein will be required. Less precise TFP can be performed in other laboratories using the camera settings and calibration provided here.

Bibliography

[1] Vilimpoc, V., Goss, L. P., "SiC-Based Thin-Filament Pyrometry: Theory and Thermal Properties," *Proceedings of the Combustion Institute*, Vol. 22, pp. 1907-1914, 1988.

[2] Vilimpoc, V., Goss, L. P., Sarka, B., "Spatial Temperature-Profile Measurements by the Thin-Filament-Pyrometry Technique," *Optics Letters*, Vol. 13, pp. 93-95, 1988.

[3] Goss, L.P., Vilimpoc, V., Sarka, B., Lynn, W. F., "Thin-Filament Pyrometry: A Novel Thermometric Technique for Combusting Flows," *Journal of Engineering For Gas Turbine sand Power,* Vol. 111, pp. 46-52, 1989.

[4] Chen, T. H., Goss, L. P., Talley, D. G., Mikolaitis, D. W., "Dynamic Stabilization Zone Structure of Jet Diffusion Flames from Liftoff to Blowout," *Journal of Propulsion and Power,* Vol. 8, pp. 548-552, 1992.

[5] Roberts, W.L., Driscoll, J. F., Drake, M. C., Goss, L. P., "Images of the Quenching of a Flame by a Vortex – To Quantify Regimes of Turbulent Combustion," *Combustion and Flame,* Vol. 94, pp. 58-69, 1993.

[6] Ferguson, C. R, Keck, J.C., "Hot-Wire Pyrometry," *Journal of Applied Physics,* Vol. 49, pp. 3031-3032, 1978.

[7] Bédat, B., Giovannini, A., Pauzin, S., "Thin Filament Infrared Pyrometry: Instantaneous Temperature Profile Measurements in a Weakly Turbulent Hydrocarbon Premixed Flame," *Experiments in Fluids,* Vol. 17, pp. 397-404, 1994.

[8] Blevins, L. G., Renfro, M. W., Lyle, K. H., Laurendeau, N. M., Gore, J. P., "Experimental Study of Temperature and CH Radical Location in Partially Premixed CH_4/Air Coflow Flames," *Combustion and Flame*, Vol. 118, pp. 684-696, 1999.

[9] Ravikrishna, R. V., Laurendeau, N. M., "Laser-Induced Fluorescence Measurements and Modeling of Nitric Oxide in Methane-Air and Ethane-Air Counterflow Diffusion Flames," *Combustion and Flame*, Vol. 122, pp. 474-482, 2000.

[10] Ji, J., Sivathanu, Y. R., Gore, J. P., "Thin Filament Pyrometry for Flame Measurements," *Proceedings of the Combustion Institute*, Vol. 28, pp. 391-398, 2000.

[11] Marcum, S. D., Ganguly, B. N., "Electric-Field-Induced Flame Speed Modification," *Combustion and Flame*, Vol. 143, pp. 27-36, 2005.

[12] Chen, T. H., Goss, L. P., "Propagation and Fractals of Turbulent Jet Flames," *Joint Propulsion Conference*, Vol. 8, pp. 16-20, 1992.

[13] Ji, J., Sivathanu, Y. R., Gore, J. P., "Thermal Radiation Properties of Turbulent Lean Premixed Methane Air Flames," *Proceedings of the Combustion Institute*, Vol. 28, pp. 391-398, 2000.

[14] Lim, J., Sivathanu, Y., Ji, J., Gore, J. P., "Estimating Scalars from Spectral Radiation Measurements in a Homogeneous Hot Gas Layer," *Combustion and Flame,* Vol. 137, pp. 222-229, 2004.

[15] Pitts, W. M., "Thin-Filament Pyrometry in Flickering Laminar Diffusion Flames," *Proceedings of the Combustion Institute*, Vol. 26, pp. 1171-1179, 1996.

[16] Pitts, W. M., Smyth, K. C., Everest, D. A., "Effects of Finite Time Response and Soot Deposition on Thin Filament Pyrometry Measurements in Time-Varying Diffusion Flames," *Proceedings of the Combustion Institute*, Vol. 27, pp. 563-569, 1998.

[17] Struk, P., Dietrich, D., Valentine, R., Feier, I., "Comparisons of Gas-Phase Temperature Measurements in a Flame Using Thin-Filament Pyrometry and Thermocouples," *American Institute of Aeronautics and Astronautics*, 41st Meeting, pp. 853, 2003.

[18] Shim, S. H., Shin, H. D., "Application of Thin SiC Filaments to the Study of Coflowing, Propane/Air Diffusion Flames: A Review of Soot Inception," *Combustion Science and Technology*, Vol. 175, pp. 207-223, 2003.

[19] Bundy, M., Hamins, A., Lee, K. Y., "Supression Limits of Low Strain Rate Non-premixed Methane Flames," *Combustion and Flame,* Vol. 133, pp. 299-310, 2003.

[20] Russo, S., Gomez, A., "Structure of Laminar Coflow Spray Flames at Different Pressures," *Proceedings of the Combustion Institute,* Vol. 29, pp. 601-608, 2002.

[21] Connelly, B. C., Kaiser, S. A., Smooke, M. D., Long, M. B., "Two-Dimensional Soot Pyrometry with a Color Digital Camera," *Fourth Joint Meeting of the U.S. Sections of the Combustion Institute*, Philadelphia, 2005.

[22] COI Ceramics Inc., www.coiceramics.com, Accessed in 2005.

[23] Klimek, R. B., Wright, T. W., Sielken, R. S., "Color Image Processing and Object Tracking System," Technical Memorandum No. 107144, NASA Lewis Research Center, 1996.

[24] Sunderland, P. B., Axelbaum, R. L., Urban, D. L., Chao, B. H., Liu, S., "Effects of Structure and Hydrodynamics of the Sooting Behavior of Spherical Microgravity Diffusion Flames," *Combustion and Flame*, Vol. 132, pp. 25-33, 2003.

[25] Bradley, D., Entwistle, A.G., "Determination of the Emissivity, for Total Radiation, of Small Diameter Platinum-l0%, Rhodium Wires in the Temperature range 600-1450 °C," *British Journal of Applied Physics*, Vol. 12, pp. 708-711, 1961.

[26] Lange, N. A., "*Lange's Handbook of Chemistry*," 4 ed., Handbook Publishers Inc., 1941.

[27] Nakai, S., Okazaki, T., "Heat Transfer from a Horizontal Circular Wire at Small Reynolds and Grashof Numbers –I Pure Convection," *International Journal of Heat Mass Transfer*, Vol. 18, pp. 387-396, 1975.

[28] Mills, A. F., *Heat and Mass Transfer*, Irwin Heat Transfer Series, p.1156, 1995.

[29] CRC Handbook of Chemistry and Physics, Weast R. C., CRC Press, West Palm Beach, p. E3, 1978.

[30] Santoro, R. J., Yeh, T. T., Horvath, J. J., Semerjian, H. G., "The Transport and Growth of Soot Particles in Laminar Diffusion flames," *Combustion Science and Technology*, Vol. 53, pp. 89-115, 1987.

[31] Sunderland, P.B., Faeth, G. M., "Soot Formation in Hydrocarbon/Air Laminar Jet Diffusion Flames," *Combustion and Flame*, Vol. 105, pp. 132-146, 1996.

[32] Lewis, B., von Elbe, G., *Combustion, Flames and Explosions of Gases, Academic Press*, Orlando, p. 720, 1987.